Using Compliant Leg Design for Impact Attenuation of Airdrop Landings of Quadruped Robots

Yeeho Song[1] and Dirk Luchtenburg[2]

Abstract— Most airdropped cargo use a combination of one or more parachutes and an impact attenuation system to land safely. The latter adds cost, weight and complexity. However, by using their legs for impact attenuation, airdropped quadruped robots may avoid the need for such a system. In this paper, various leg configurations for attenuating impact of airborne landings were studied and tested. Using simple lumped element models for simulation and analysis, a quadruped robot with a three-segment leg was designed and built. This model was validated with experiments with a small scale 20 cm-tall test robot. During the experiments, the test robot experienced $7.7 \times 10 \, m/s^2$ or 7.9 g-acceleration when dropped from height of 37.85 cm. This result is much better than the result of $1.4 \times 10^2 \, m/s^2$ or 14.7 g-acceleration when dropped at 10% of the original height with the same robot equipped with rigid legs. Such compliant leg design could be potentially used for impact attenuation of airdrop landings of robots five times larger.

I. INTRODUCTION

Parachutes are used worldwide in both civilian and military sectors to land a variety of cargo and personnel into hostile territory, disaster zones, and even on the surface of Mars. However, as a parachute can only decelerate cargo to its terminal velocity, airdropped cargo is usually packed with additional impact attenuation system such as retrorockets, airbags, and / or cushioning materials. However, such a system leads to additional weight, cost, and effort to pack and unpack cargo and hide the system from enemy detection if necessary.

On the other hand, personnel airdrop requires no additional impact attenuation system. Using a technique called Parachute Landing Fall (PLF), a human jumper first land on one's toes, and using the compliance of one's knees, absorbs the impact of landing by folding one's leg and gently rolling over to distribute the impact sequentially along the side of his body. This allows a jumper to land safely without the need for additional impact attenuation system to prevent a severe damage to one's musculoskeletal system. If such method can be applied to quadruped robots, they too may be able to land safely without any additional impact attenuation system.

Moreover, this application may also improve the mobility of quadruped robots. Unlike those by airbags or retrorockets, impact attenuation by the use of legs can be repeatedly used, allowing such a system to be applied for locomotion as well. For example, instead of trying to find a sloped detour, a quadruped robot could simply jump down from high places, improving its mobility in mountainous and / or

urban terrain. Likewise, such compliant legs could be used to better attenuate impact from running at high speeds.

Therefore, in this paper, we study various leg configurations and their impact attenuation performances. In particular, we aim to design a leg configuration for a quadruped robot that is capable of landing an airdropped robot safely without the need for an additional impact attenuation system.

II. LITERATURE STUDY

Currently, there are three major techniques for impact attenuation of robotic landings: 1) active damping, 2) passive damping or use of compliant legs, and 3) control of a robot's posture to guide the fall. Active damping relies on feedback control of robot's actuators to control limb posture in real time in order to attenuate impact. While active damping provides a method of attenuating impact for robots with rigid actuators, active damping alone with such actuators is not effective unless the robot can accurately predict its impact, as pointed out by Dallali [1]. Otherwise, impact on rigid legs will be too short that a robot's controller will not be able to react in time to attenuate impact properly.

In contrast to rigid actuators, compliant actuators connect actuators and limbs with springs, dampers, or strings to allow limbs to move during impact without applying controls. As noted by Pratt [2] and Radkaha[3], compliant actuators can not only allow energy storage, but also allow for better shock tolerance. For example, Anathanarayanan [4] used compliant leg designs to reduce the stress on robot's leg structures from walking by 59%, while Niiyama [5] used pneumatic actuators and leaf springs to design a pair of compliant legs which allowed a 10 kg robot to be drooped from height of 1 m without damaging any of its components.

A robot's impact attenuation performance can also be improved by controlling the robot's posture. For example, Fujiwara's robot [6] can roll when falling to minimize stress on robot's structure while Wang [7] designed a robot to shift its torso's center of mass to change the direction of the fall. Likewise, Yun [8] programmed a robot to control its posture of limbs to avoid falling onto nearby objects.

III. APPROACH

A. Mission Profile

As there are currently no quadruped robots used in airdrop missions, typical mission parameters for this paper were derived from specifications of existing pieces of hardware fulfilling similar roles. The weight and size of the dropped robot is comparable that of Boston Dynamics' BigDog [9]. As this robot and its successors are designed to carry load

Department of Mechanical Engineering, Cooper Union, New York, NY 10003, USA [1]yeehosong21@gmail.com [2]dluchten@cooper.edu

in rough terrain alongside infantry, BigDog is closest to the role of being airdropped into hostile territory and disaster zones. The descent rate of the robot was set to 6.1 m/s, which is the descent rate of a MC1-1B personnel parachute [10]. Although a G-14 cargo parachute might be a more likely candidate, its descent data is not publicly available.

B. Scaling and Concept Study

Our experiments were conducted with 1:5 scale test robots, since repeatedly dropping a robot as big and heavy as BigDog, at a descent rate of 6.1 m/s, was difficult to realize. The descent rate v, or the impact speed, was also scaled down to allow for lower drop heights. The average acceleration $\bar{a}$ (deceleration) during a landing is given by:

$$\bar{a} = \frac{\Delta \text{KE}}{mx} = \frac{v^2}{2x}, \qquad (1)$$

where ΔKE is the change in kinetic energy during a landing, m the mass of the robot, and x the vertical folding length of the robot's legs during a landing. Note that $x \leq L$ where L is the maximum allowable vertical folding length (height of the robot). For both scales, the minimum average acceleration $\bar{a}_{min} = v^2/2L$ was about the same. For a given impact speed v and average acceleration $\bar{a}$, Eq. 1 determines how much the robot's legs compress during an impact (Δx). However, the leg design can be optimized to lower the peak acceleration value.

We conducted an airdrop pilot study with a 20 cm-tall robot weighing 850 g equipped with an active damping system for impact attenuation. The robot's impact speed was 2.7 m/s. The test results showed that the entire landing usually took less than 300 ms, with the peak acceleration occurring within 20 ms of the first contact with the ground. Due to the mechanical lag of the servos, the robot's leg posture could not be adjusted fast enough to effectively reduce the peak acceleration during the landings. In addition, the servos had the tendency to freeze upon impact, rendering active damping ineffective. In fact, the best results were obtained when active damping was disabled and the robots legs were set such that it landed on two side legs and rolled over.

C. Design considerations & requirements

Based on the results of the pilot study, we decided to use compliant legs for impact attenuation. Four different leg configurations were considered: a one-segment (1S), a two-segment compliant structure (2SCS), a two-segment compliant joint (2SCJ), and a three-segment (3S) leg, see Figs. 1, 2, 3, and 4 respectively. All leg designs are required to meet the following:

1) The legs can support a standing robot.
2) The legs can generate a static crawl gait.
3) the legs can sufficiently attenuate the impact of an airdrop.

The first requirement implies a spring will be compressed to exert force F_{base} for each leg configuration to support's robot weight and make the robot stand up straight. Standing straight means that the robot's feet are directly located under the hip joints, and the joints are 20 cm off the ground, see Fig. 8.

The second requirement states that the legs must be able to generate a static stable gait (crawl). In particular, the legs should be able to move forward and backward by 6.6 cm while maintaining a height of 20 cm from hip to ground. In order to lift the feet off the ground while walking, knee servos with pulleys are used for the 1S, 2SCJ, and 3S configurations, see Figs. 1, 3, and 4. A knee servo with a pulley pulls a string that loads (compresses) a spring. This load needs to be within design specifications of the employed servos. For the 2SCS configuration, knee servos are used to rotate the knee directly, see Fig. 2. While walking, one or two feet might be off the ground, so we also require that the springs should be able to support half of the robot's weight.

The third requirement highlights the fact the the robot is designed for airdrop missions. The legs are designed to minimize the peak acceleration of the robot's body during landing to at least to $120\,m/s^2$ or 12.3 g's (70% of the acceleration for the case which the robot was set to roll over upon impact). In order to reduce the acceleration, the springs are set to be uncompressed when the robot is airdropped to fully utilize the length of legs for impact attenuation. This requires that the knee servos have enough range of motion for 1S, 2SCJ and 3S configurations. The hip servos, for all configurations, do not move during a landing.

D. Analysis Methods

For ease of analysis, the following assumptions were made for the analysis of each leg configuration:

- Quasi-static analysis is used to derive the forces and equations of motion.
- Legs are considered to have negligible mass compared to that of the entire robot. For the test robot, each leg weighed 41 g out of total weight of 830 g for the robot.
- The deformation of the structural members and rigid joints are negligible compared to that of the springs.
- The springs are perfectly linear and only compress and stretch in the lengthwise direction. For the test robot, this is enforced by a cylindrical braces for the springs, see Fig. 8.
- The effect of friction (damping) is not considered.
- The springs are uncompressed (fully extended) during drops.

E. One-Segment (1S) and Two-Segment Compliant Structure (2SCS) legs

The one-segment leg was designed like a pogo stick, see Fig. 1. It does not have a knee and its length is directly affected by a spring, which its length is set by pulling a string that is connected to a pulley.

The two-segment compliant structure (2SCS) leg configuration has hips and knees that are directly actuated. The lower half of the leg is replaced by a spring. Although the 1S and 2SCS are two different configurations, they can be analyzed in the same way.
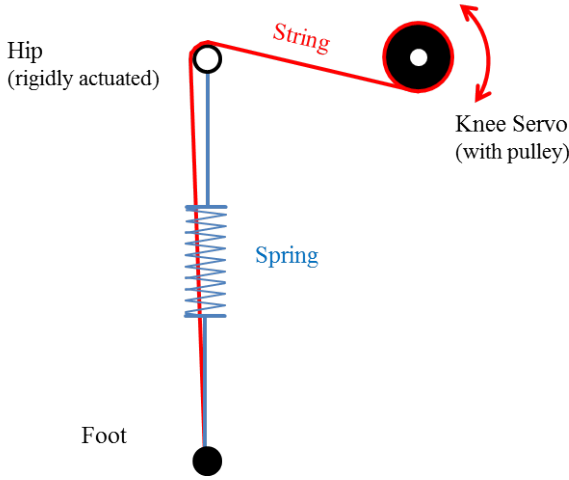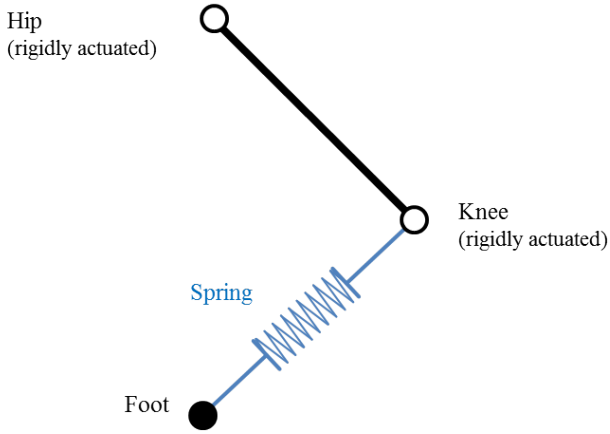
Fig. 1. One-segment leg (1S) configuration.

Fig. 2. Two-segment compliant structure (2SCS) leg configuration.

The spring force, $F_{s,k}$, follows from Hooke's law:

$$F_{s,k} = k(\ell_{s0} - \ell_s) \qquad (2)$$

where k is the spring constant, ℓ_{s0} is the uncompressed length of the spring, and ℓ_s the actual length of the spring at a given time. In order to compress the spring, the knee servo must be able to exert a torque τ_{req} given by:

$$\tau_{req} = F_{s,k}\, r_p, \qquad (3)$$

where r_p is the radius of the pulley.

The equation of motion for the robot during landing is obtained as follows. By assuming that all kinetic and gravitational energy of the robot is absorbed by its four springs as potential energy, we obtain:

$$a = -\frac{4kx}{m} - g, \qquad (4)$$

where a is the acceleration of the robot, x the vertical folding length of the leg during impact, m the mass of the robot, k the spring constant, and g the gravity constant.

F. Two-Segment Compliant Joint (2SCJ) Leg

The two-segment compliant joint (2SCJ) leg configuration has hips that are directly actuated and knees that are compliant, see Fig. 3.
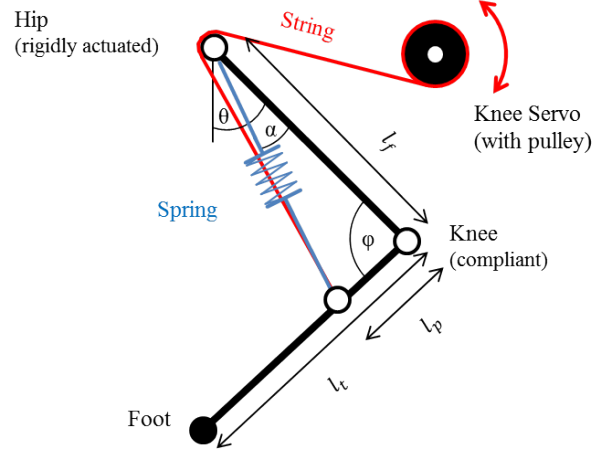

Fig. 3. Two-segment compliant joint (2SCJ) leg configuration.

The legs need to support the weight of the robot while walking. Using a quasi-static analysis, the spring force $F_{s,req}$ is calculated as follows:

$$F_{s,req} = \frac{mg}{2}\,\frac{\ell_t \sin(\theta + \varphi)}{\ell_p \sin(\varphi + \alpha)}, \qquad (5)$$

where m is the mass of the robot, g the gravity constant, and other geometric variables defined in Fig. 3. The torque required for the knee servo to pull the string and compress the spring can be computed using Eq. 3.

The equation of motion for the robot during landings is obtained in a similar way:

$$a = \frac{4F_{s,k}}{m}\,\frac{\ell_p \sin(\varphi + \alpha)}{\ell_t \sin(\theta + \varphi)} - g, \qquad (6)$$

where $F_{s,k}$ is as defined in Eq. 2.

G. Three-Segment (3S) Leg

The three-segment (3S) leg configuration has hips that are directly actuated, and knees and ankles that are compliant, see Fig. 4.

Using a quasi-static analysis, the spring force $F_{s,req}$ required to support the weight of the robot during walking is calculated as follows:

$$F_{s,req} = \frac{mg}{2}\,\frac{\sin(\theta + \varphi)}{\sin(\alpha)}, \qquad (7)$$

where, as before, m is the mass of the robot, g the gravity constant, and other variables are defined in Fig. 4.

The following equation of motion is used during landings:

$$a = \frac{4F_{s,k}}{m}\,\frac{\sin(\alpha)}{\sin(\theta + \varphi)} - g, \qquad (8)$$

where $F_{s,k}$ is defined in Eq. 2. As above, the torque required by the knee servo is computed using Eq. 3.
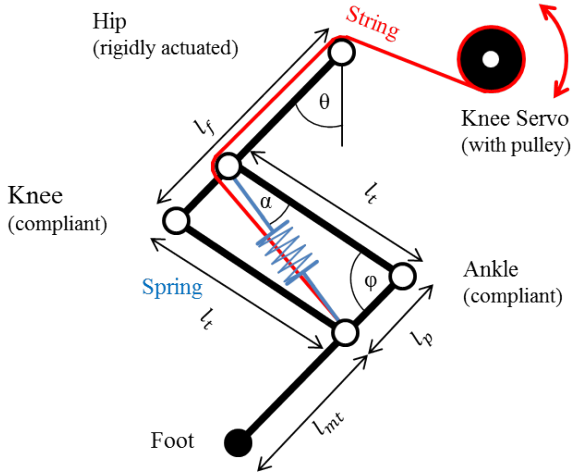
Fig. 4. Three-segment (3S) leg configuration.

H. Design Optimization and Construction

In this section, we analyze the four leg configurations from the previous sections for feasibility in our airdrop mission. As stated in Sec. III-C, the legs must support the robot's weight, provide locomotion and sufficiently attenuate the impact of an airdrop. Therefore, each configuration was first designed for walking and subsequently tuned for impact attenuation performance.
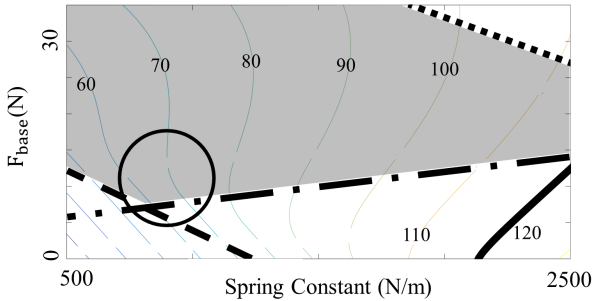

Fig. 5. Allowable spring choice and settings for the 3S leg configuration. The contour lines indicate the maximum acceleration during landing (in m/s^2).

The design procedure is explained using the 3S leg configuration, see Fig. 5. This plot shows the spring force F_{base} (the base force required for the robot to stand up straight, $20\,cm$ above ground, see Sec. III-C) vs. the spring stiffness k, or the spring constant. Based on the design requirements, the gray region indicates the allowable choices for the spring stiffness and the base force.

In the region above the dot and dash line the springs can support the robot's weight during walking. Impact attenuation requires that the robot comes to a full stop before the springs are fully compressed which restricts the allowable region to the right of the dashed line. We require that the maximum acceleration during landing is less than $120\,m/s^2$ or 12.3 g's which corresponds to the region left of the continuous line. The maximum servo torque set by

our hardware is indicated by the dotted line (region left of it is allowable). We decided to keep F_{base} as low as possible, since larger values generally require larger springs. Given these constraints, we can optimize the 3S configuration for impact attenuation. The circle in Fig. 5 represents the most favorable spring settings, and indicates that we can limit the maximum acceleration to $60 \sim 70\,m/s^2$ or $6 \sim 7$ g's
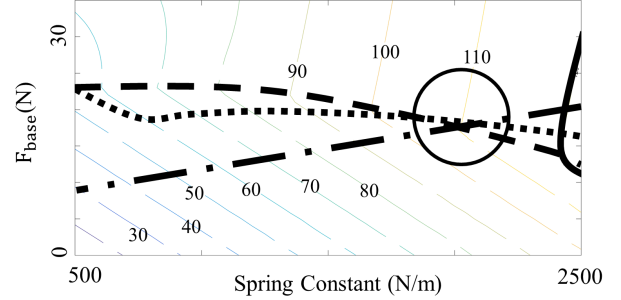

Fig. 6. Allowable spring choice and settings for the 2SCJ leg configuration. The contour lines indicate the maximum acceleration during landing (in m/s^2).

We can apply the same procedure to the other leg configurations. Fig. 6 shows that the optimal minimum acceleration for the 2SCJ configuration is at around $110\,m/s^2$ or 11 g's, much higher than that of 3S configuration. This is likely because the 3S legs have two segments that fold during landing, whereas the 2SCJ legs only have one. Thus, the latter fold over a shorter distance. As a result, the 2SCJ springs must be stiffer in order to decelerate the body while covering less vertical distance. In addition, the 2SCJ springs require a longer range of motion than 3S, which increases minimum size of pulley to cover the range of motion, thus leading to greater load on knee servos and less faborable leg performance compared to that of 3S.
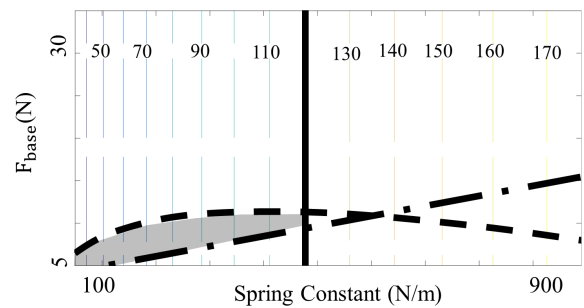

Fig. 7. Allowable spring choice and settings for the 1S and 2SCS leg configurations. The contour lines indicate the maximum acceleration during landing (in m/s^2).

Fig. 7 shows the allowable specifications for the springs of the 1S and 2SCS leg configurations when disregarding the maximum servo torque. These configurations look promising as they shows that the acceleration during landing can be made relatively low.

However, a 1S configuration requires a larger range of spring motion than a 3S configuration, and consequently the

load on the knee servo is higher. This can be dangerous when one operates close to the servo's limit, and the robot might not be able to overcome disturbances such as sticky surfaces, or internal friction. Also, to match the 3S's result of 60 ~ 70 m/s^2 or 6 ~ 7 g's, the springs must have a range of motion of 0.09 m, nearly half height of the robot from hip to ground.

Given the constraints of cost-effective rapid prototyping, we decided to build our test robot of 3D-printed polylactic acid (PLA) parts, as it is relatively straightforward to construct a 3S configuration with 3D printed plastic parts. As it is more difficult to construct the required long legs for the 1S configuration while maintaining structural integrity to withstand impact with the ground, such design was not pursued. As for 2SCS designs, while the configuration would bypass this issue with the main loads on the knee servos, the issue of providing enough range of motion remains. Fully compliant legs, such as carbon fiber blade feet, could be utilized, but this was beyond the scope of this research. Therefore, we chose the 3S leg configuration for our airdrop mission, see Figs. 4 and 8.

While we note that BigDog is made out of metal parts, the PLA parts of our 3S legs are relatively rigid compared to the spring and the joints as metal parts would be in a full scale robot. For actual construction, practical considerations resulted in a slight deviation from the optimal design point. One was finding the right spring from various vendors, and the other was designing an appropriate spring-cylinder structure that would have enough range of motion and structural integrity. The torque load on the hip servos was limited so as not to exceed the servo specifications. Table I lists the dimensions of the test robot shown in Fig. 8.

TABLE I

SPECIFICATIONS OF THE TEST ROBOT

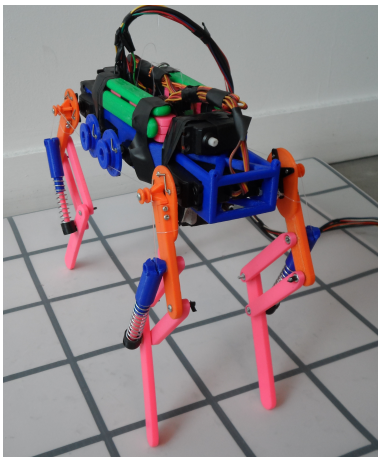| Length	220 mm
Height	200 mm
Weight	830 g
Length of ℓ_f / ℓ_t / ℓ_{mt} / ℓ_p	80 mm / 80 mm / 80 mm / 30 mm

Fig. 8. Quadruped test robot with a 3S leg configuration.

IV. EXPERIMENT

The drop tests for the robot were conducted from a height of 37.85 cm in order to achieve a (scaled) descent rate or impact speed of 2.7 m/s. The robot was dropped with different hip joint angles ($\theta = 30°$, $37.5°$, and $45°$), see Fig. 4, to validate the simulation model. For each angle setting 30 ~ 40 drop tests were conducted. The acceleration of the robot was measured by a LSM303 3-axis accelerometer installed on the main body of the robot. The sensor had a sampling rate of 80.85 Hz and the standard deviation of sensor measurements was 2%. To avoid cases where the robot did not landed straight, causing the spring cylinders to be misaligned and being locked in place, videos were taken of each drop test for analysis.

To compare the effectiveness of compliant legs versus rigid legs, additional drop tests were conducted with the springs locked in place. The legs were fixed in a standing position, with the feet directly under hips. To avoid breaking the robot with such rigid legs, drop tests were conducted at reduced testing heights of 10, 20, and 70% of the original test height of 37.85 cm.
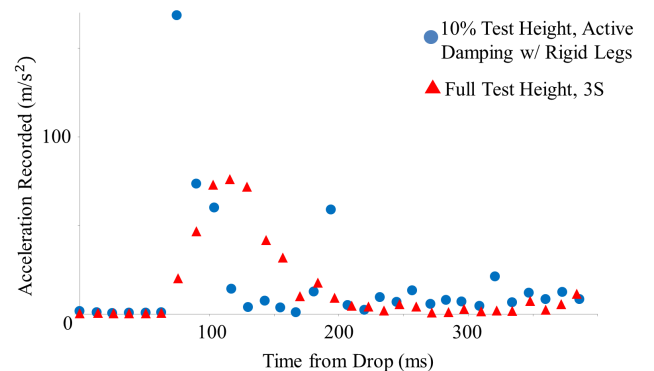
V. RESULTS AND DISCUSSION

Fig. 9. The acceleration of the robot during airdrop tests (in m/s^2)

As shown in Fig. 9, compliant legs attenuate the impact of a landing much better than rigid legs by smoothing out the sharp peak over a longer time duration.

TABLE II

MAXIMUM ACCELERATION DURING LANDING WITH COMPLIANT LEGS
(IN m/s^2 (G'S))

θ (°)	Simulation	Experiment	Std.Dev.	Difference(%)
30	7.6×10	7.7×10 (7.9)	8.8 (0.89)	0.90
37.5	7.8×10	7.9×10 (8.1)	6.9 (0.70)	5.11
45	8.2×10	8.3×10 (7.4)	2.9 (0.30)	1.33

In Table II simulation results are compared with averaged experimental data, showing a good agreement. This indicates that our simple lumped model can predict the motion of the robot during landing up to a some accuracy. The actual results are slightly higher than the simulation results, which

is likely due to friction which was unaccounted for in the model. For example, misaligned spring cylinders can create a huge amount of friction strong enough to prevent the legs from folding properly upon impact. The results also indicate that even when the robot is built, hip opening angles, θ, can be adjusted to adjust the impact attenuation performance.

TABLE III

Maximum acceleration during landing with rigid legs ((in m/s^2 (g's))

Test Height (%)	Experiment results	Std.Dev.
10	1.4×10^2 (14.7)	33 (3.4)
20	Leg Broke	N/A
70	Leg Broke	N/A

Table III lists the maximum acceleration during a landing with fixed (locked-up) legs. Comparing these results with those in Table II, we see that compliant legs lead to a maximum acceleration that is about half of that of rigid legs dropped from a 10% of the full height.

TABLE IV

Ratio of successfully landing with all feet contacting ground as desired

Tested Robot	# Drops	# Successes	Success rate
Robot from Pilot Study	31	14	45%
Actual Test Robot	40	29	73%

Table IV compares successful landings of the robot from the pilot study with active damping to the robot with the 3S compliant leg configuration. For such cases, a landing is successful when the robot lands on all its feet, distributing the load across all of its legs. It can be seen that the probability of the compliant legs landing in the desired posture is 60% better than that of the rigid legs. This could be from that the passive compliant legs can adjust posture following the robot's movement and orientation, thus balancing faster and more reliably than legs with only active damping.

VI. CONCLUSION

We designed and analyzed leg configurations for a quadruped robot that were optimized for both walking and impact attenuation for airdrop missions. Based on a pilot study which showed active damping to be ineffective for such cases, we decided to use compliant legs for impact attenuation. In particular, we considered four leg configurations: a one-segment (1S), a two-segment compliant structure (2SCS), a two-segment compliant joint (2SCJ), and a three-segment (3S) leg. Given the design constraints and analysis with simple lumped element models, the 3S configuration was selected. A robot was build out of 3D-printed plastic parts. A series of experimental scaled drop tests was conducted, which showed that a 3S compliant leg configuration allows a $20\,\mathrm{cm}$-tall quadruped robot to safely land from a height of $37.85\,\mathrm{cm}$ while experiencing an acceleration of 77

m/s^2 or $7.9\,\mathrm{g}$'s. The same robot dropped with fixed legs at 10% of the original height experienced a twice larger peak acceleration. The impact attenuation performance of compliant legs was also shown better compared to active damping or control of posture on a quadruped robot with rigid legs. In addition, a robot with compliant legs was much more likely to land on its four feet. A comparison between experimental and simulation results revealed good agreement, and it seems that the motion of the robot is captured adequately by simple lumped element models.

The simple methods used in this paper could be potentially applied to robots that are much larger than the ones we used for this research, and it would be interesting to see if our modelling approach scales well. Our study only considered vertical drops and future studies should include horizontal movement to simulate, for instance, a robot on a parachute descent that is being pushed by wind during the descent. Study on addition on incorporation of non-linearly elastic members such as carbon fiber feet could also be conducted in the future, especially with the 2SCS configuration.

Part of this work was originally presented as an IEEE undergraduate student conference paper at the 2016 IEEE MIT Undergraduate Research Technology Conference.

ACKNOWLEDGMENT

REFERENCES

[1] H. Dallali, P. Kormushev, N. G. Tsagarakis and D. G. Caldwell, "Can active impedance protect robots from landing impact?," *2014 IEEE-RAS International Conference on Humanoid Robots,* Madrid, 2014, pp. 1022-1027.

[2] G. A. Pratt and M. M. Williamson, "Series elastic actuators," *Proceedings 1995 IEEE/RSJ International Conference on Intelligent Robots and Systems. Human Robot Interaction and Cooperative Robots,* Pittsburgh, PA, 1995, pp. 399-406 vol.1.

[3] K. Radkhah and O. von Stryk, "A study of the passive rebound behavior of bipedal robots with stiff and different types of elastic actuation," *2014 IEEE International Conference on Robotics and Automation (ICRA),* Hong Kong, 2014, pp. 5095-5102.

[4] A. Ananthanarayanan, M. Azadi and S. Kim, Towards a bio-inspired leg design for high-speed running, *Biosinpiration & Biomimetics,* Volume 7, Number 4, Bioinspiration & Biomimetics, 2012

[5] R. Niiyama, Y. Kuniyoshi, Design of a musculoskeletal athlete robot : a biomechanical approach, *Proceedings 12th International Conference on Climbing and Waling Robots and the Support Technologies for Mobile Machines (CLAWAR 2009),* Istanbul, Turkey, 2009, pp.183-180.

[6] K. Fujiwara textitet al., "The first human-size humanoid that can fall over safely and stand-up again," textitProceedings 2003 IEEE/RSJ International Conference on Intelligent Robots and Systems (IROS 2003) (Cat. No.03CH37453), 2003, pp. 1920-1926 vol.2.

[7] J. Wang, E. C. Whitman and M. Stilman, "Whole-body trajectory optimization for humanoid falling," *2012 American Control Conference (ACC),* Montreal, QC, 2012, pp. 4837-4842.

[8] S. k. Yun, A. Goswami and Y. Sakagami, "Safe fall: Humanoid robot fall direction change through intelligent stepping and inertia shaping," *2009 IEEE International Conference on Robotics and Automation,* Kobe, 2009, pp. 781-787.

[9] M. raibert, K. Blankesppor, G. Nelson, R. Playter and the BigDog Team, BigDog, the rough-terrain quadruped robot, *Proceedings 17th IFAC World Congress,* Seoul, Korea, 2008, pp.10822-10825, Volume 41, Issue 2.

[10] Mills Manufacturing, "MC1-1B/E Parachute Assembly", Mills Manufacturing, Web. 1 September 2016